

Design of polymeric auxetic matrices for improved mechanical coupling in lead-free piezocomposites

Jagdish A Krishnaswamy^{1,4} , Federico C Buroni², Roderick Melnik^{1,3},
Luis Rodriguez-Tembleque³  and Andres Saez³

¹ MS2Discovery Interdisciplinary Research Institute, Wilfrid Laurier University, 75 University Ave W, Waterloo, Ontario, N2L 3C5, Canada

² Department of Mechanical Engineering and Manufacturing, Universidad de Sevilla, Camino de los Descubrimientos s/n, Seville E-41092, Spain

³ Department of Continuum Mechanics and Structural Analysis, Universidad de Sevilla, Camino de los Descubrimientos s/n, Seville E-41092, Spain

E-mail: ajagdish@wlu.ca

Received 28 October 2019, revised 13 February 2020

Accepted for publication 10 March 2020

Published 1 April 2020



Abstract

While lead-free piezocomposites offer an environmentally friendly solution to mechanical sensing and energy harvesting, they lag state-of-the-art lead-based materials in terms of performance. It is therefore important to develop new material designs to bridge this performance gap. Considering composites where rigid piezoelectric inclusions are embedded in soft matrices, a major cause of poor performance is weak coupling of applied strains to the inclusions. We show here that by designing matrices with negative Poisson's ratios (auxetic matrices) it is possible to considerably improve this coupling. We first demonstrate this concept using a matrix which is inherently auxetic where we show an improvement of 40%–50% in the piezoelectric response. Based on the observations made, we develop a scalable design for auxetic matrices using conventional non-auxetic polymeric materials. This is done by embedding rigid auxetic structures in softer matrices. We show that with such designed auxetic matrices, which are amenable to fabrication through 3D printing, it is possible to achieve considerably larger piezoelectric response with a significant retention of the matrix softness. Particularly, we show that auxetic designs can show piezoelectric enhancements exceeding 300% compared to non-auxetic reference designs having similar a non-auxetic rigid backbone of similar volume as the auxetic backbone. Therefore, the use of matrices with negative Poisson's ratios is a promising design avenue to decouple mechanical coupling of strain to inclusions and matrix hardness. This strategy can pave way to design of softer piezocomposites with superior responses employing only structured polymeric materials without the use of expensive nanomaterials.

Keywords: piezoelectric composite, finite element analysis, auxetic materials, polycrystal, multiscale design and homogenization, 3D printing

(Some figures may appear in colour only in the online journal)

1. Introduction

Piezoelectric composites are materials that bring together the favorable mechanical properties of a matrix material, which is

mostly non-piezoelectric, and the piezoelectric properties of embedded inclusions [1, 2]. The choice of materials and structures allows a range of possible mechanical and piezoelectric properties including the design for desired anisotropy of properties [3, 4]. The possibility to tune the piezoelectric properties through the tuning of the composite structure at

⁴ Author to whom any correspondence should be addressed.

multiple length scales is made feasible by the recent developments in scalable manufacturing processes such as 3D printing [3, 5–7]. The recent focus is on the development of composites based on lead-free materials [8, 9]. Although investigation of environmentally friendly composites based on lead-free materials constitutes an active area of research, the performance of these materials considerably lags behind lead-based materials [9]. It is, therefore, important to conceive new designs, considering the possibility of structured materials and new manufacturing techniques, to develop superior lead-free piezocomposite materials.

A major source of performance loss in such composites, especially when rigid piezoelectric inclusions are embedded in soft matrices, is the weak coupling of applied mechanical stimuli to the inclusions which results in a very weak piezoelectric response [10]. It is known through earlier research that carbon-based nanofillers can address this issue by hardening the matrix material and by efficiently channeling the applied mechanical stimuli into the inclusions [10, 11]. However, most of these designs, for example that involve a matrix modified by the addition of carbon nanotubes (CNTs), entail considerable hardening of the matrix, making the design less suitable to applications requiring flexible devices [12]. For example, applications involving implantable electronic devices, wearable devices and circuits, and so on, pose the requirement of superior piezoelectric performance while requiring the retention, to the best possible extent, of the ‘softness’ of the matrix material without the use of expensive nanomaterials. The development of new material designs using commonly available polymeric materials, which can be fabricated using emerging manufacturing technologies such as 3D printing, form the central premise of this work.

Here, we show that the decoupling between the matrix stiffness and efficiency of mechanical coupling to the inclusions can be brought about using auxetic matrices, or matrices with a negative Poisson’s ratio. Unlike conventional materials, auxetic materials possess structures that allow them to spatially expand in a direction normal to an applied tensile stress [13]. While isotropic materials can have a minimum Poisson’s ratio of -1 , there is no such lower limit for anisotropic materials [13]. This means that a variety of anisotropic structures can be designed with a large range of Poisson’s ratios. Many such structures, including chiral, antichiral, re-entrant topologies have been investigated [14–19] in design and fabricated by methods such as 3D printing [5]. The use of structured materials possessing such unusual properties offers new avenues to tune material properties and performance beyond the possibilities of state-of-the-art strategies. The role of auxeticity in the enhancement of piezoelectric response has received some attention in the form of designs involving simple bimorphic [20] or simple 1–3 architectures [21, 22] which have shown some promise in improving the mechanical coupling to the piezoelectric components of the setup. However, efforts in imparting an auxetic structure to the piezoelectric material itself do not show an encouraging results towards enhanced piezoelectric response [23]. Therefore, the main point of investigation here

will be that of developing an auxetic design for the matrix in which randomly shaped piezoelectric lead-free inclusions are embedded, as will be the case in a practical composite material.

Here, we present a novel material design possibility where using auxetic matrices—either inherently auxetic or optimally structured for auxetic behaviour—it is possible to bring about large improvements in the piezoelectric response, due to improved mechanical coupling of applied strain to the piezoelectric inclusions embedded in the matrix. A further goal of the work is to study how the polycrystallinity of the piezoelectric inclusions can be tuned to further improve the piezoelectric response of the composites based on the auxetic matrices. We first demonstrate that inherently auxetic polymeric matrices can help improve ambient-to-inclusion strain coupling leading to significant improvements in the piezoelectric response. Secondly, we develop a novel design for auxetic matrices by embedding auxetic stiff polymeric structures within soft polymeric matrices. The polymeric materials used here are not inherently auxetic and the structures investigated are amenable to additive manufacturing processes. We further show that these engineered auxetic matrices can also lead to a significant boost in the piezoelectric response.

In the following sections, we will first provide details of the electro-elastic model used to design and analyse the composites and subsequently discuss the findings of the analysis.

2. Electro-elastic model and material considerations

In this section, we will briefly explain the coupled electro-elastic model used in our analysis, the boundary conditions employed, and the material properties used for the study. Section 2.1 describes the electro-elastic model including the governing laws and constitutive relations. Section 2.2 provides a brief overview of the materials involved in the investigation and details of their properties.

2.1. The electro-elastic model

The piezoelectric behaviour of a composite is determined by a linear coupling between strain and the electric field, expressed by the following phenomenological relations [22, 24, 25]

$$\sigma_{ij} = c_{ijkl}\epsilon_{kl} - e_{kij}E_k, \quad (1a)$$

$$D_i = \epsilon_{ij}E_j + e_{ijk}\epsilon_{jk}, \quad (1b)$$

where σ_{ij} and ϵ_{kl} are the stress and strain tensor components, respectively, and E_i and D_i are the electric field and flux density components, respectively. These fields are coupled through the material properties which include the elastic coefficients c_{ijkl} , the permittivity ϵ_{ij} , and the piezoelectric coefficients e_{ijk} . These equations are further subject to conditions of equilibrium and Gauss’s law [22, 24, 25], given by

$$\sigma_{ij,j} - F_i = 0, \quad (2a)$$

$$D_{i,i} = 0, \quad (2b)$$

where F_i refers to the body force components, which are zero in this study.

Table 1. Electro-elastic material properties of the matrix materials and piezoelectric inclusions.

Material property	Polyethylene (PE) [27–28]	PEGDA [29, 30]	Epoxy—LY5052 ([31] and datasheets)	Single crystal BaTiO ₃ [26, 32]
Elastic coefficients (Moduli in Pa)				
c_{11}	$\lambda_m + 2\mu_m$	$\lambda_m + 2\mu_m$	$\lambda_m + 2\mu_m$	275.1×10^9
c_{13}	λ_m	λ_m	λ_m	151.55×10^9
c_{33}	$\lambda_m + 2\mu_m$	$\lambda_m + 2\mu_m$	$\lambda_m + 2\mu_m$	164.8×10^9
c_{44}	μ_m	μ_m	μ_m	54.3×10^9
Young's modulus, E_m	100×10^6	1×10^6	1×10^9	—
Poisson's ratio, ν_m	Auxetic Nonauxetic	−0.32 0.2	0.35	0.35
Relative permittivity				
ϵ_{11}/ϵ_0	2.3	10	3.5	1970
ϵ_{33}/ϵ_0	2.3	10	3.5	109
Piezoelectric coefficients (Cm ^{−2})				
e_{31}	—	—	—	−2.69
e_{33}	—	—	—	3.65
e_{15}	—	—	—	21.3

Further, the strains are related to the displacement components u_i as

$$\epsilon_{ij} = \frac{1}{2}(u_{i,j} + u_{j,i}), \quad (3a)$$

and the electric field is related to the electric potential V as

$$E_i = -V_{,i}. \quad (3b)$$

The composite architecture, which will be subject to these equations, can take multiple forms. It can be a representative volume element (RVE) of an auxetic structure of the matrix material or it can be an RVE of a piezoelectric composite comprising of both the homogenized matrix and inclusion materials. Given this variability, we will describe the RVE architectures investigated, along with the boundary conditions employed, in the relevant parts of the section on the results. The phenomenological relations given by equation (1), subject to the governing differential equations given by equation (2) and the assumption-based relations (equation (3)) are solved using finite element analysis.

2.2. Materials and properties

In this section, we briefly discuss the materials involved in this study and their electro-elastic properties. First, we will look at the polymeric matrix materials investigated here. Particularly, the first part of the results (section 3.1) investigates the auxetic and nonauxetic forms of polyethylene matrices. The second part of the results (section 3.2) investigates engineered auxetic matrices made of structures of conventional non-auxetic materials. These materials include a soft base matrix, PEGDA, with an embedded auxetic structure made of a relatively stiffer epoxy, LY5052 (as a representative example). The piezoelectric inclusion material is polycrystalline BaTiO₃ which is a well-understood lead-free piezoelectric material. The electro-elastic coefficients of polycrystalline BaTiO₃ are obtained from single crystal data as reported in [26], following orientational averaging. Table 1

summarizes all the electro-elastic properties of interest for the matrix and the single crystal BaTiO₃ that are used in the analysis. In the table, the terms λ_m and μ_m refer to the Lamé's parameters which describe the elastic properties of the isotropic polymeric materials employed in the study. These are given by

$$\lambda_m = \frac{E_m \nu_m}{(1 + \nu_m)(1 - 2\nu_m)}, \quad \mu_m = \frac{E_m}{2(1 + \nu_m)}, \quad (4)$$

where E_m and ν_m are the Young's modulus and the Poisson's ratio of the material.

As mentioned earlier, a polycrystalline material model [26] is used to obtain the electro-elastic coefficients of polycrystalline BaTiO₃ from single crystal data. The polycrystallinity is quantified by a parameter α which would depend on the condition of crystal quality, poling, and other processing parameters. The limits $\alpha \rightarrow 0$ and $\alpha \rightarrow \infty$ correspond to the single crystal with all the dipoles oriented along the same direction and a disoriented polycrystal with all the dipoles oriented in random directions, respectively. Intermediate values of α represent polycrystals with a net orientation along a preferred axis which is the direction along which the composite is poled by application of electric fields (the c -axis of the BaTiO₃ unit cell). The electro-elastic properties of polycrystalline BaTiO₃, obtained from [26], are given in appendix A1. The composites are assumed to be poled along the x_3 direction and hence the net orientation of the c -axis of the BaTiO₃ inclusions will be along the x_3 direction, with some random deviations determined by the value of α . Although we have assumed that all the polycrystals have a mean orientation along the same direction (i.e. the poling direction), in reality, the percentage poling factor which measures this effectiveness of poling along a direction, in composites, is slightly lesser than unity [33]. Therefore, the assumption we make about the net orientation of all the polycrystals being along the x_3 direction is similar to practical conditions in a piezocomposite. The exact details of the RVE

architecture, matrix microstructure and so on will be provided in the results section.

3. Results and discussion

The approach taken in this analysis is to analyse the possible role of matrix auxeticity in enhancing the piezoelectric response. This implies that the studies involve a comparison of matrices which are both non-auxetic and auxetic. We will start with a proof-of-concept in section 3.1, where we will compare a non-auxetic and an auxetic matrix possessing similar elastic moduli. This will help identify distinctly the role of the negative Poisson's ratio in determining the performance of the piezoelectric composite. In this section, we consider polymer matrices possessing auxeticity as a result of the specific processing steps employed, and there might be limitations on the range of tunability in the elastic properties (i.e. Young's modulus and the Poisson's ratio). Therefore, in the subsequent section (section 3.2), we develop scalable matrix geometries where geometrically induced auxeticity in the matrix can be introduced by using manufacturing techniques such as 3D printing. This will allow a design-based tunability in the elastic and auxetic properties of the matrix while using simple commercially available non-auxetic polymeric materials amenable to 3D printing. Therefore, we will proceed from a proof-of-concept demonstration to a more refined and controlled manufacturable design for auxetic matrices for piezocomposites.

3.1. Improved mechanical coupling using inherently auxetic matrices

In this section, we will carry out initial analyses on polymer matrices which can possess negative Poisson's ratios as a result of a complex microstructure that can form during the manufacturing process. As an example, we consider polyethylene (PE). Depending on the specific nature of processing, the polymer can possess either an auxetic or a nonauxetic behaviour. This depends on whether the process allows the formation of a microstructure that allows such a behaviour [27, 28]. However, both the variants of the polymer possess similar Young's moduli [27, 28]. From the perspective of piezocomposite design, this allows a fair comparison to distinctly identify the effects of auxeticity in the matrix on the piezoelectric response. Table 1 lists the Young's moduli and the Poisson's ratio of non-auxetic and auxetic PE. We employ a composite architecture with a small inclusion concentration of $V_{BTO} = 6.3\%$, for this proof-of-concept investigation. The RVE employed for this analysis is shown in figure 1(a), along with the boundary conditions BC1 and BC2 in figures 1(b) and (c), respectively. These are boundary conditions that enforce tensile loads to obtain the effective properties. It is also possible to obtain the effective properties using periodic boundary conditions on the RVE. Although it is suggested that a periodic boundary conditions can lead to better prediction of effective properties [34, 35], we note that unless the RVE is treated as a unit cell [36], given its present

size, different boundary conditions lead to similar effective properties [37]. Following this observation, we use the uniform tensile load boundary conditions in this work. The details of the effective properties that are extracted from these boundary conditions are provided in the appendix A2. In short, we are interested in the calculation of the effective piezoelectric coefficients e_{31}^{eff} and e_{33}^{eff} of the composite which are obtained from boundary conditions BC1 and BC2, respectively. Also, we are interested in calculating the effective elastic coefficients of the composites c_{11}^{eff} , c_{13}^{eff} , and c_{33}^{eff} . BC1 is used to calculate c_{11}^{eff} , BC2 is used to calculate c_{33}^{eff} , while c_{13}^{eff} can be calculated using either of the boundary conditions. These are standard boundary conditions used for the computation of effective homogenized electro-elastic properties [22, 24, 25]. The RVE is assumed to be a square with sides $a_m = b_m = 50 \mu\text{m}$ and the randomly shaped and randomly positioned inclusions are approximately $5 \mu\text{m}$ across. We apply a small boundary strain of $\bar{\epsilon}_a = 1 \times 10^{-6}$ for both the boundary conditions.

We look at the effective piezoelectric coefficients e_{31}^{eff} and e_{33}^{eff} of the composites in figures 2(a) and (d). We see the auxetic matrix leads to a better piezoelectric response in both the cases. Since, both the matrices have similar Young's moduli and permittivities, the enhancement is clearly due to the auxeticity of the second matrix. Particularly, we note that the volume-averaged axial strains in the inclusions ($\langle \epsilon_{11} \rangle_{inc}$ and $\langle \epsilon_{33} \rangle_{inc}$ in the evaluation of e_{31}^{eff} and e_{33}^{eff} , respectively, with the subscript *inc* referring to the inclusion average), normalized with respect to the applied boundary strain $\bar{\epsilon}_a$ (see figures 1(a), (b)) undergo a significant enhancement. This implies that the applied axial strain is transferred more effectively into the inclusion in the presence of an auxetic matrix, as suggested by figures 1(b) and (f) in the case of the boundary conditions BC1 and BC2, respectively.

Secondly, we also note that when a tensile axial strain is applied, the compressive strain in the inclusions, in the direction normal to the axis of the tension, increases considerably in the presence of the auxetic matrix (figures 2(c) and (e) corresponding to boundary conditions BC1 and BC2, respectively). This is due to the auxetic effect: when a tensile strain is applied, the auxetic matrix tends to expand in the direction normal to the strain, leading to an increased compressive strain on the inclusion. Although the nature of the strains $\langle \epsilon_{11} \rangle_{inc}$ and $\langle \epsilon_{33} \rangle_{inc}$, under a given condition of loading (boundary condition BC1 or BC2), are of opposite signs, they lead to flux generation in the same direction because of the opposite signs of the piezoelectric coefficients e_{31} and e_{33} of the inclusions. Therefore, the improvements in the coupling of applied strain into the inclusion and the improvement in the compressive strain in the inclusion in the direction normal to the stimulus reinforce piezoelectric flux generation and are responsible for the observed improvement in the piezoelectric response.

From the preceding analysis, to understand the source of enhancement and its nature of dependence on the polycrystallinity of the inclusions, we need to evaluate the improvements in the inclusion averaged strains. We further

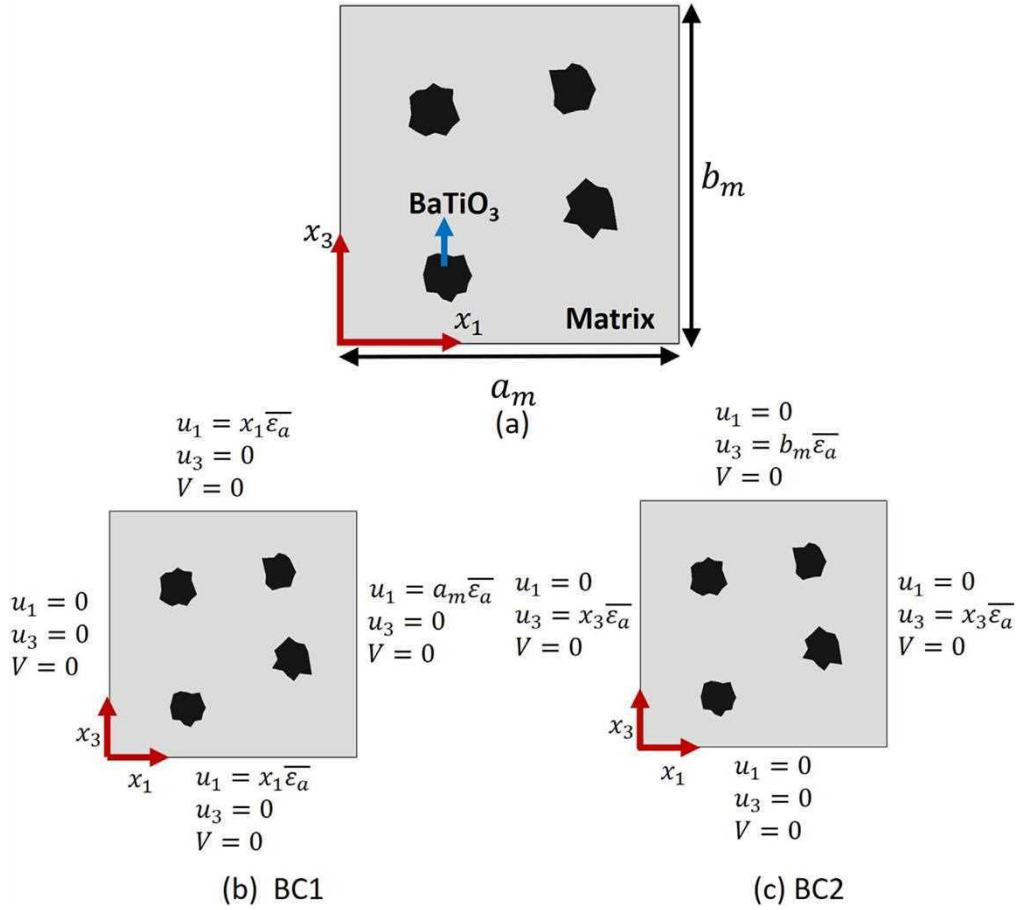


Figure 1. (a) The piezocomposite RVE with dilute piezoelectric inclusion concentration, $V_{\text{BTO}} = 6.3\%$, used to study the effects of an inherently auxetic isotropic matrix. (b) and (c) show the boundary conditions BC1 and BC2 applied on the RVE to extract the effective electro-elastic coefficients of the composite.

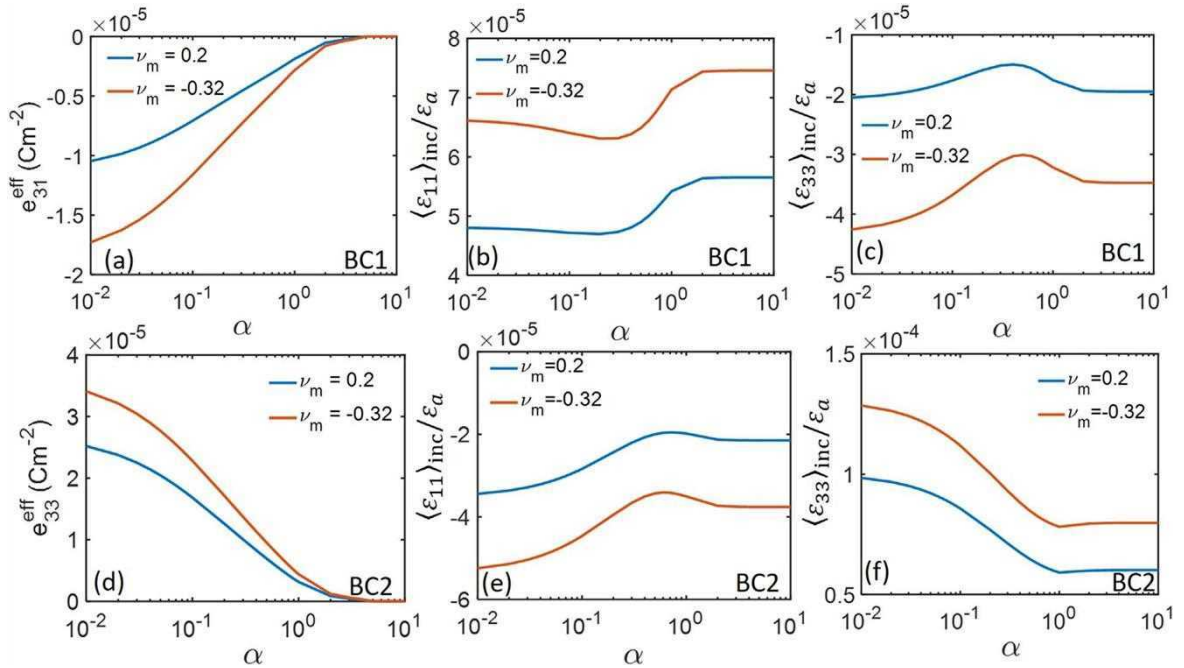


Figure 2. The effective piezoelectric coefficients of the proof-of-concept composite architecture shown in figure 1 are shown in (a) and (d), corresponding to boundary conditions BC1 and BC2, respectively. (b), (c) and (e), (f) show the inclusion averaged strains in the non-auxetic and auxetic designs corresponding to the boundary conditions BC1 and BC2, respectively, as indicated inside each subfigure.

plot the relative improvements (absolute values) in the average strains within the inclusions. These are given by

$$\Delta \varepsilon_{11} = \left| \frac{\langle \varepsilon_{11} \rangle_{inc}^{M_{aux}} - \langle \varepsilon_{11} \rangle_{inc}^{M_{ref}}}{\langle \varepsilon_{11} \rangle_{inc}^{M_{ref}}} \right|, \quad (5)$$

$$\Delta \varepsilon_{33} = \left| \frac{\langle \varepsilon_{33} \rangle_{inc}^{M_{aux}} - \langle \varepsilon_{33} \rangle_{inc}^{M_{ref}}}{\langle \varepsilon_{33} \rangle_{inc}^{M_{ref}}} \right|,$$

where the superscripts M_{aux} and M_{ref} indicate the type of matrix—auxetic and the reference nonauxetic matrix, respectively, and the subscripts *inc* indicate that volume averaging has been carried out over the inclusions.

We use absolute values because we have seen that for a given boundary condition, BC1 or BC2, the inclusion averaged strains ε_{11} and ε_{33} are of opposite signs, and we are interested only in magnitude of their relative improvements. This is again because, as already discussed, an elongation along a direction and a compression in the normal direction generate flux components in the same direction, owing to the form of the piezoelectric coefficients.

We see two distinct trends here. In the case of e_{31}^{eff} , the auxeticity-induced enhancement in the inclusion-averaged strains is significant for lower values of α (figure 3(a)), indicating that the improvement in the effective coefficient e_{31}^{eff} is better in single-crystal-like inclusions. On the other hand, on observing the enhancements in the inclusion-averaged strain, with the composite subjected to boundary condition BC2 (specific to evaluation of the e_{33}^{eff}), we see that while there are significant enhancements in coupling of applied strain into the inclusions, the enhancements are more pronounced for higher values of α (figure 3(b)). This implies that the enhancement is higher for polycrystalline inclusions. This behaviour is also reflected in the relative improvements in the effective piezoelectric coefficients, as shown in figure 3(c) where we plot the relative improvements Δe_{31} and Δe_{33} in the effective coefficients e_{31}^{eff} and e_{33}^{eff} of the composite based on the auxetic matrix, with respect to the reference design based on the non-auxetic matrix. Even with small inclusion concentrations, improvements exceeding 50% are possible when auxetic matrices are used. Secondly, while the improvement in e_{31}^{eff} is better in single-crystal-like inclusions, the improvements in e_{33}^{eff} are better in polycrystalline inclusions. This way, the introduction of auxeticity into the matrix, through synthesis-controlled microstructures, makes it possible to break the bottlenecks involved in effectively coupling the applied mechanical stimuli into the inclusions. Further, the auxeticity-induced strain amplification in the inclusion has a non-trivial dependence on the polycrystalline state of the inclusions.

3.2. Piezoelectric enhancement using designed auxetic matrix structures

In the previous section, we saw that while maintaining the same elastic modulus, a negative Poisson's ratio in an isotropic matrix can lead to considerably better mechanical coupling from the ambient source of stimuli into the embedded inclusions in the composite. However, it is to be noted that the auxeticity observed

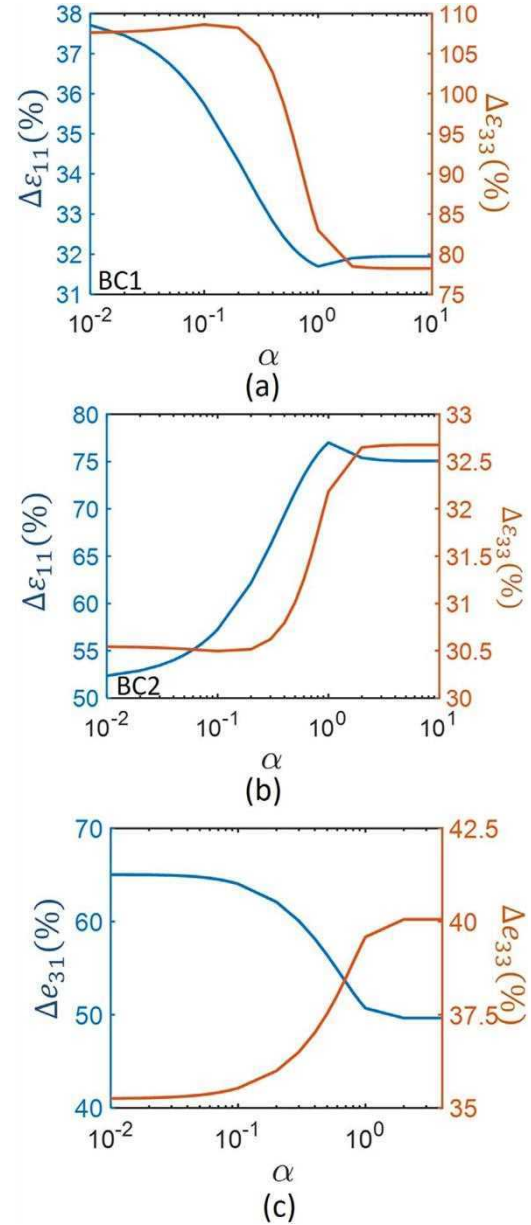


Figure 3. (a), (b) Show the relative improvements in the inclusion averaged strains with boundary conditions BC1 and BC2, respectively, as a function of the polycrystalline index α . In (a), $\Delta \varepsilon_{11}$ and $\Delta \varepsilon_{33}$ correspond to improvements in tensile and compressive components of the respective strains ε_{11} and ε_{33} in the inclusions, and in (b) $\Delta \varepsilon_{11}$ and $\Delta \varepsilon_{33}$ correspond to improvements in compressive and tensile components, respectively. This follows from the nature of the applied boundary conditions. (c) shows the relative improvements in the effective piezoelectric coefficients e_{31}^{eff} and e_{33}^{eff} as a function of α .

in such materials is sensitive to the microstructure, which in turn has a sensitive dependence on the processing parameters [27, 28]. Such manufacturing or synthesis processes might not be compatible with all polymeric matrices of interest. Secondly, such processes might not provide flexibility in terms of tuning the Poisson's ratio in an anisotropic sense, which would be important for many applications [3]. The goal of this section is to investigate whether auxeticity can be imparted to standard non-auxetic polymeric materials by embedding geometrically tailored rigid

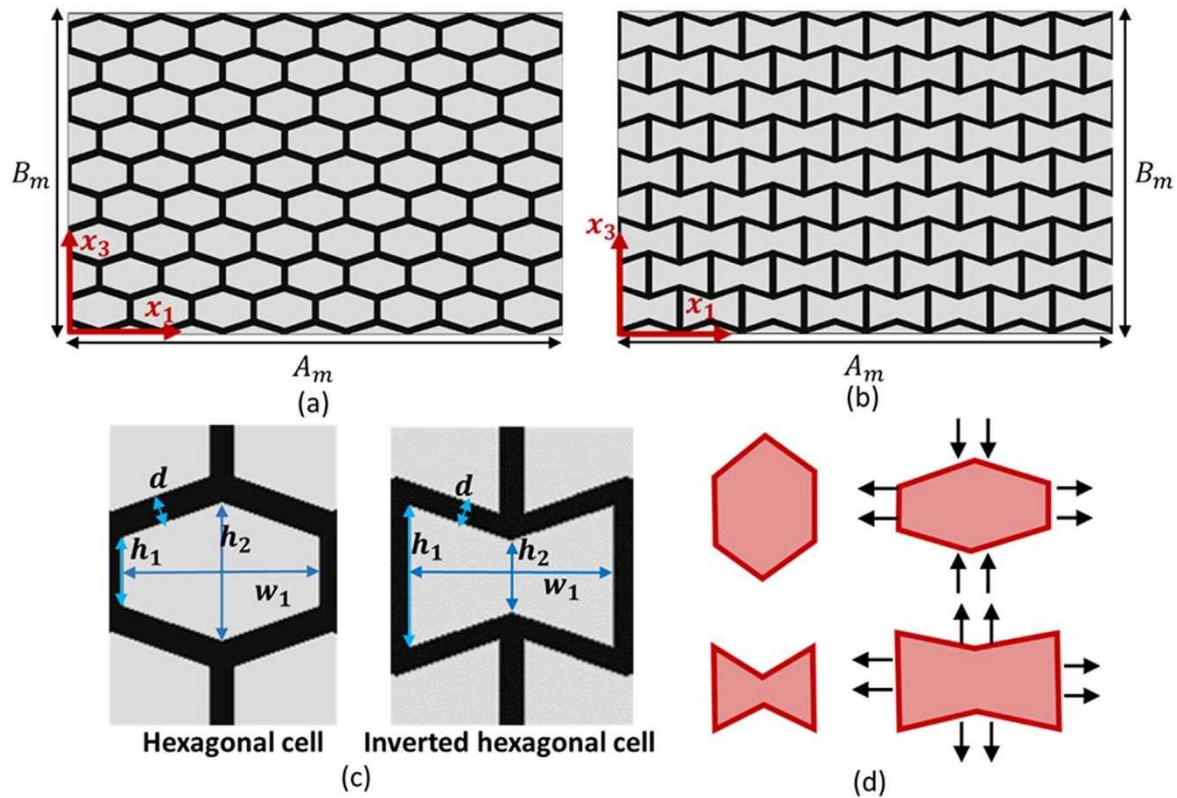


Figure 4. (a) and (b) Show the RVEs of the proposed matrices comprised of a soft host matrix (in gray) in which a relatively rigid polymeric backbone (either (a) hexagonal (nonauxetic) or (b) Inverted hexagonal (auxetic)) is embedded. (c) shows the geometrical parameters which define the unit cell of the backbone. (d) illustrates how the hexagonal and the inverted hexagonal structures behave as nonauxetic and auxetic structures, respectively, with the arrows indicating the direction of net strain.

polymeric microstructures in a standard polymeric matrix. We hypothesize that when a relatively rigid auxetic microstructured backbone is embedded in a much softer polymer, the auxeticity of the backbone can be imparted to the bulk of the matrix on an average. We investigate two such microstructured backbones having the same volumes, shown in figures 4(a), (b). The two matrices have periodically arranged hexagonal and inverted-hexagonal unit cells, respectively, as shown in the figure 4(c). The free standing cellular structures of the network of hexagon and the inverted-hexagon structures are well studied and often are representative examples of non-auxetic and auxetic structures having similar volumes [14, 15]. The auxeticity in the inverted hexagon arises solely due to the structure: on application of tensile stress on the sides of the inverted hexagon, the ribs forming the remaining sides move out leading to an apparent-expansion, or a net-negative Poisson's ratio (schematic in figure 4(d)), although the constituent material can be a standard non-auxetic material [38]. These structures considered here have orthotropic symmetry with the out-of-plane axis serving as the direction of extrusion of the in-plane geometry illustrated in figures 4(a), (b). As shown in these figures, the matrix RVEs are rectangles with sides A_m and B_m . The backbones consist of periodically repeating units in a hexagonal lattice. The values of these geometric parameters for both the matrices are given in table 2. The parameters h_1 , h_2 , w , and d are chosen by scaling down experimentally verified auxetic geometries as illustrated in [5]. It is clear from table 2, that the nonauxetic and auxetic

Table 2. Geometric parameters of the microstructured composite matrix shown in figure 4.

Parameter	Non-auxetic matrix (figure 4(a))	Auxetic matrix (figure 4(b))
A_m	80 μm	52 μm
B_m	80 μm	52 μm
h_1	3 μm	6 μm
h_2	6 μm	3 μm
w	9 μm	9 μm
d	1 μm	1 μm

backbones differ only in their values of h_1 and h_2 —the auxetic backbone is generated by simply interchanging the parameters h_1 and h_2 of the nonauxetic architecture. Therefore, the volume fraction of the backbone within the softer matrix is constant for both the nonauxetic and the auxetic cases and is equal to approximately 27%.

The elastic properties of the base matrix (PEGDA) and the material comprising the backbone (epoxy—araldite LY5052) are shown in table 1. These materials are chosen such that the backbone is considerably rigid compared to the matrix, so that the elastic properties of the backbone can be efficiently transferred to the matrix, with the effective elastic properties of the composite matrix being dominated by the properties of the relatively rigid backbone. Secondly, from the point of view of applications, the use of a soft matrix is important in the

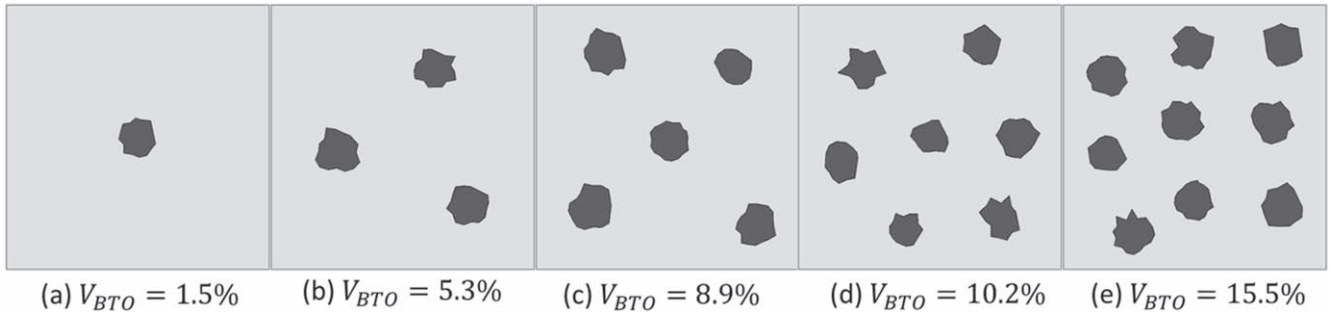


Figure 5. (a)–(e) The RVEs with the homogenized microstructured matrices and single crystal BaTiO₃ inclusions. The randomly shaped objects are BaTiO₃ inclusions which are embedded in the square matrix with sides $a_m = b_m = 500 \mu\text{m}$.

perspective of flexible and wearable electronic devices and circuits. Soft matrices, which are important for such applications, have disadvantages: they exhibit very weak mechanical coupling of the applied stimulus into the significantly harder piezoelectric inclusion. Conventional methods of improving this coupling has been to harden the entire matrix using nanoadditives such as carbon nanotubes, graphene, and so on [10]. However, this leads to significant hardening of the whole composite and could render the material too rigid for applications requiring very soft devices. Secondly, the conventional approach makes use of nanomaterials which could be an expensive design strategy. Therefore, the approach taken here aims at (a) partially hardening the matrix by introducing a microscale rigid network, (b) enhancing the mechanical coupling into inclusions making the rigid network auxetic. In doing so we make use of only polymeric materials which could be 3D printed and not nanomaterials, the synthesis or manufacturing of which could pose scalability issues.

Using the effective homogenized elastic and dielectric properties of the matrix obtained using the boundary conditions explained in appendix A3, we carry out simulations on piezoelectric RVEs shown in figures 5(a)–(e), with different dilute inclusion concentrations. These simulations use the homogenized properties of the designed matrices and further the randomly shaped piezoelectric inclusions are of rough sizes around $50 \mu\text{m}$, which is five times larger than the unit cells of the designed matrices. Considering the larger inclusion sizes which need to exceed the feature sizes of the microstructured matrices for a homogenized model for the matrix to be a valid approximation, the RVEs studied here are larger than those shown in figure 1. Therefore, the sides of the RVE are $a_m = b_m = 500 \mu\text{m}$. The applied boundary strains are small and given by $\bar{\epsilon}_a = 1 \times 10^{-6}$. The RVEs are subject to the same boundary conditions illustrated in figures 1(b), (c), i.e. BC1 and BC2, respectively, to obtain the effective elastic and piezoelectric coefficients. Further, the inclusions are assumed to be single crystals, for simplicity.

The simulated effective elastic coefficients of the composites with these two matrices are shown in figures 6(a)–(c), as a function of the inclusion concentration V_{BTO} . In both the composites, the microstructured matrices cause approximately 2–3 orders of magnitude increase in the effective elastic coefficients, implying a slight hardening of the composite. This matrix is considerably softer compared to a homogeneous matrix made of only the material comprising the backbone, which would have effective coefficients that are further 2–3 orders of magnitude higher than that of the microstructured composite architectures

[39]. Secondly, the matrix with the inverted-hexagonal network has a negative c_{13}^{eff} which confirms the auxetic nature of the material and our hypothesis that a rigid backbone with auxetic structure can transfer its properties to the whole matrix. It is further to be noted that this coefficient becomes more negative on addition of more inclusions, indicating an inclusion-driven increase in the auxetic effect of the piezocomposite. More importantly, the matrix with the inverted hexagonal network has smaller elastic coefficients compared to the matrix with the hexagonal network. Intuitively, we would expect that a stiffer matrix (i.e. the non-auxetic matrix, here) would lead to a better piezoelectric response. However, on observing the simulated effective piezoelectric coefficients e_{31}^{eff} and e_{33}^{eff} in figures 6(d) and (e), respectively, we observe that the auxetic matrix outperforms the non-auxetic design. While the auxetic matrix gives a slightly better e_{31}^{eff} than the nonauxetic architecture, this improvement is much more significant in the case of e_{33}^{eff} , with the auxetic matrix giving a piezoelectric response which is roughly around 300% better compared to the non-auxetic matrix. To understand the source of such significant improvements, we plot the inclusion averaged strain components in figure 7, where figures 7(a), (b) correspond to the boundary condition BC1, and figures 7(c), (d) correspond to the boundary condition BC2, corresponding to the evaluation of e_{31}^{eff} and e_{33}^{eff} , respectively. We expect the trends of the strains to be different than in the case of auxetic-PE matrices seen in the previous section, because these designed architectures are anisotropic, and their behaviour can considerably deviate from that of isotropic matrices. In the case of the e_{31}^{eff} , which is evaluated by the application of boundary condition BC1, we see that the average value of the strain ϵ_{11} , in the inclusions, is slightly higher in the case of the nonauxetic matrix, compared to the auxetic matrix (figure 7(a)).

The average value of the strain ϵ_{33} shown in figure 7(b) shows that the inclusions undergo net compression in the case of both the designed matrices. However, the inclusions in the auxetic composite experience a higher compressive strain, leading to higher flux generation in the $-x_3$ direction, contributing constructively to the flux generated by the ϵ_{11} strain component, also in the $-x_3$ direction. Therefore, from figures 7(a) and (b), we see that the nonauxetic and the auxetic matrices compete in flux generation, which leads to only a slight net improvement in the effective piezoelectric coefficient e_{31}^{eff} of the composite. This trend, however, changes in the case of the effective coefficient e_{33}^{eff} . The average value of the strain component ϵ_{33} , corresponding to the axis of applied elongation,

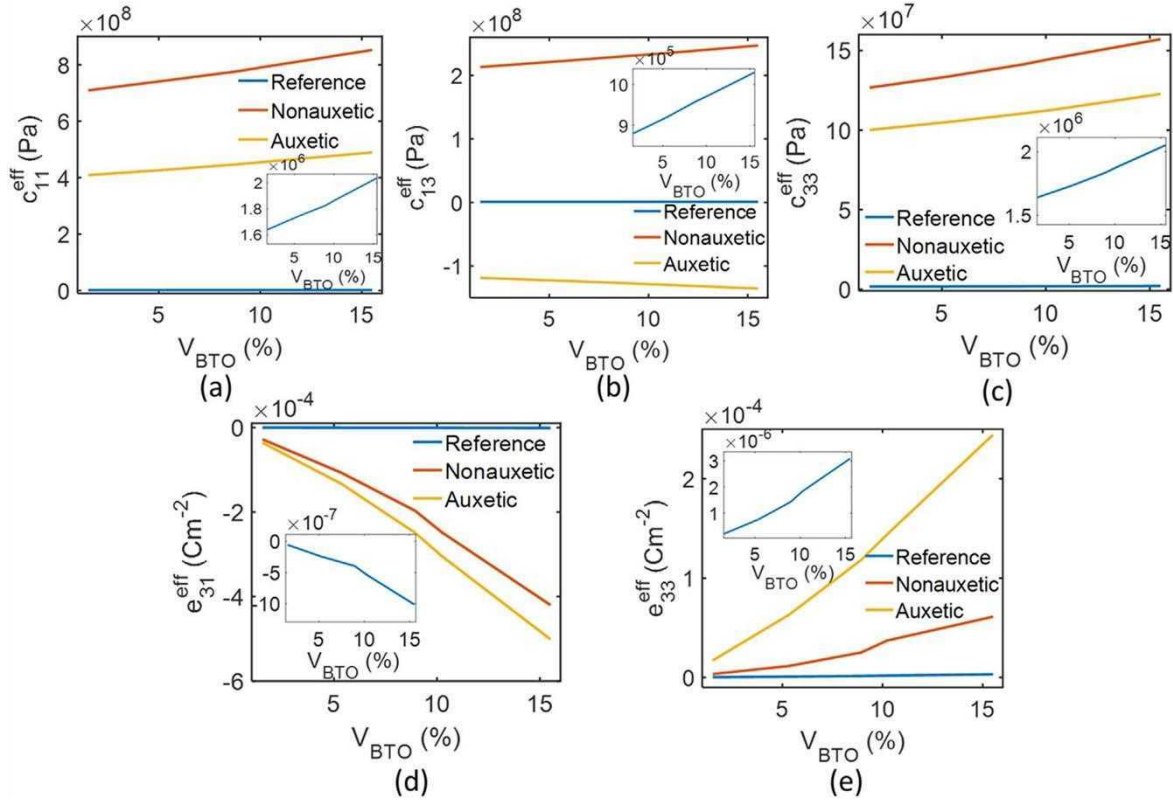


Figure 6. (a)–(c) The simulated effective elastic coefficients of the piezoelectric composites with BaTiO₃ inclusions embedded in the reference, nonauxetic (figure 4(a)), and the auxetic (figure 4(b)) matrices. (d), (e) The effective piezoelectric coefficients of the reference, nonauxetic, and auxetic composites. For better clarity, the insets in the figures show the magnified plots in the case of the reference composite architecture.

within the inclusions, is higher in the auxetic matrix, as seen in figure 7(d).

Also, in the case of the inclusion average of the strain component ϵ_{11} which is in the direction normal to applied elongation, the nonauxetic matrix exhibits a net tensile strain and the auxetic matrix shows a net compressive strain. It is precisely this compressive strain that is required in order to generate electric flux along the same direction as that generated by the net ϵ_{33} . This resulting configuration of average inclusion strains leads to the auxetic matrix resulting in a significantly higher flux generation compared to the nonauxetic matrix. Therefore, in the case of auxetic matrices with tailored geometry, there is a sensitive link between the strain distributions/strain-amplifications within the inclusions and the auxetic geometry of the matrix. Through a proper selection of geometry, it is possible to obtain dramatic improvements in mechanical coupling of applied strains to the inclusions, and hence in the piezoelectric flux generated. Also, the anisotropy allows selective enhancement of certain piezoelectric components, which further allows a degree of freedom in tuning the anisotropy of the piezoelectric response of the composite, which is an important problem of practical importance [3]. Importantly, the design of such matrices is scale invariant unless we are concerned with very small length scales where flexoelectric effects due to strain gradients or large strain conditions where nonlinear electrostrictive effects become significant. This means that if we are in the design regime where linear piezoelectricity accurately describes the material behaviour, the matrix geometry can be

scaled to larger or smaller sizes and the effective properties will remain the same.

In conclusion, it is possible to develop scale-invariant designs for auxetic matrices using nonauxetic polymeric materials, which can enhance the performance of lead-free piezocomposites through strain-amplification within the piezoelectric inclusions. This enhancement mechanism stems purely from structuring of standard polymeric materials, without the use of expensive nanomaterials and the designed demonstrated here are also amenable to fabrication through methods such as 3D printing. Through proper selection of auxetic structures that are embedded in the matrix, it is possible to obtain selective enhancement of certain piezoelectric coefficients in the composite, making this design suitable for the design of composites with tunable piezoelectric anisotropy.

4. Conclusions

We have demonstrated a new design for lead-free piezocomposites wherein we show that an auxetic matrix, either inherently auxetic or made auxetic by imparting an optimal material structure, can bring about significant enhancements in the piezoelectric response. This is due to improved mechanical coupling of the applied strain to the embedded piezoelectric inclusions. Firstly, we demonstrated this phenomenon in a proof-of-concept design using an inherently auxetic polymer matrix where around 50% improvement in the piezoelectric response

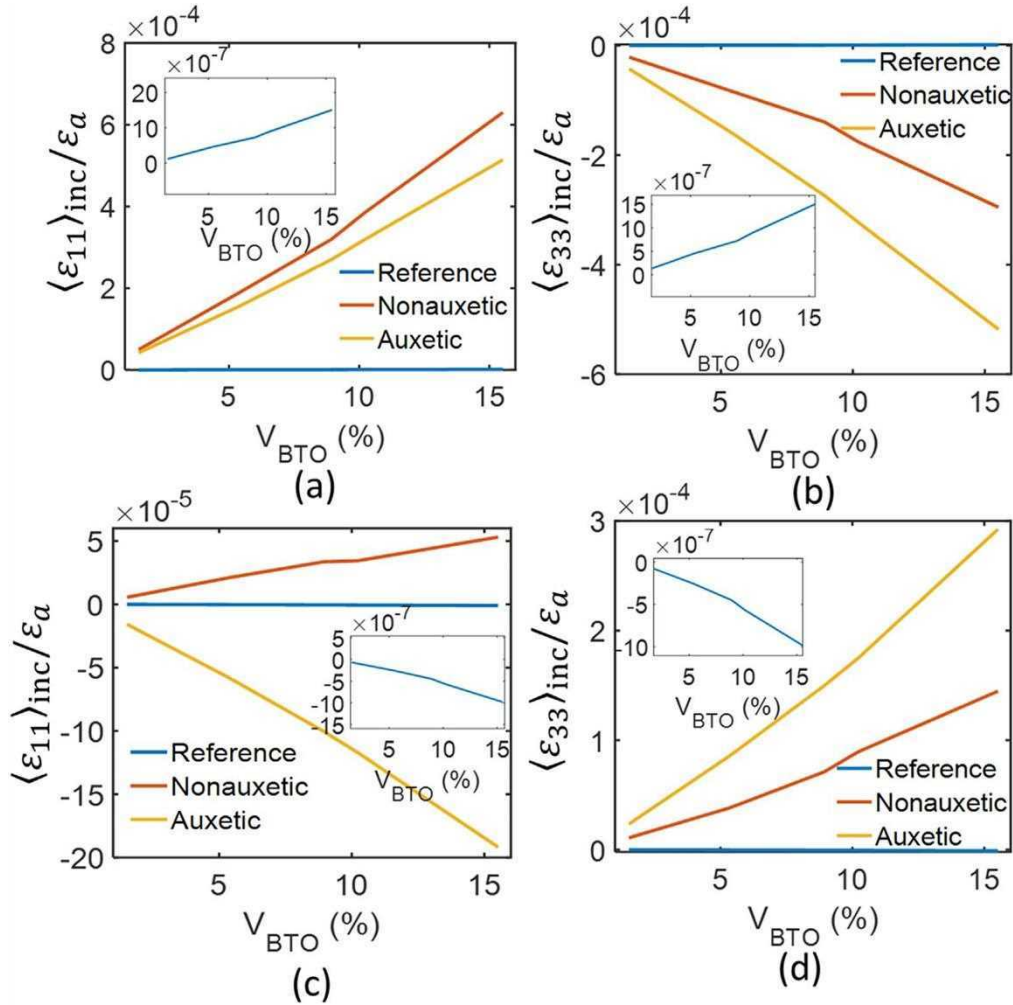


Figure 7. (a) and (b) Show the inclusion averaged strains relative to the applied interfacial strain ϵ_a with the composites subjected to boundary condition BC1 to evaluate e_{31}^{eff} of the composite, (c) and (d) show the corresponding values of the same parameters, with the boundary conditions BC2 used to evaluate e_{33}^{eff} of the composite. The insets show magnified plots for the reference composite architecture, for better clarity.

was observed even with dilute inclusion concentrations. Following this observation, we designed auxetic matrices by embedding a rigid polymeric auxetic inverted-hexagonal network within a softer matrix. Using this matrix, we further demonstrated significant enhancements in piezoelectric performance compared to a similar nonauxetic matrix. Further, we also show that the polycrystalline orientation distribution of the piezoelectric inclusions can be further tuned to bring about larger improvements in the response of the piezocomposites based on auxetic matrices. In summary, this work demonstrates the design of structured polymeric auxetic matrices as a new avenue to boost piezocomposite performance, without the use of nanomaterials. Importantly, in these investigations, we note that the auxetic matrices lead to improved performance with a considerable retention of the softness of the composite, thus decoupling matrix hardness and piezoelectric performance which is otherwise a problem with conventional methods using nanomodified matrices. This makes possible the design of soft piezocomposites with superior performances making the design strategy attractive to applications in wearable, implantable, and flexible electronics.

Furthermore, the ability to selectively enhance certain piezoelectric coefficients considerably more than the others, through the designs discussed here, it is possible to conceive strategies to tailor the piezoelectric anisotropy of the composites which is an important aspect for many applications requiring directional response. In addition to being scale-invariant and to using commonly available polymeric materials, the design also lends itself to state-of-the-art scalable manufacturing techniques such as 3D printing, thus having a significant potential technological impact.

Acknowledgments

This work was supported by the Ministerio de Economía y Competitividad of Spain and the European Regional Development Fund under projects RTI2018-094945-B-C21 and DPI2017-89162-R. The financial support is gratefully acknowledged. RM and AKJ are also grateful to the NSERC and CRC program for their support.

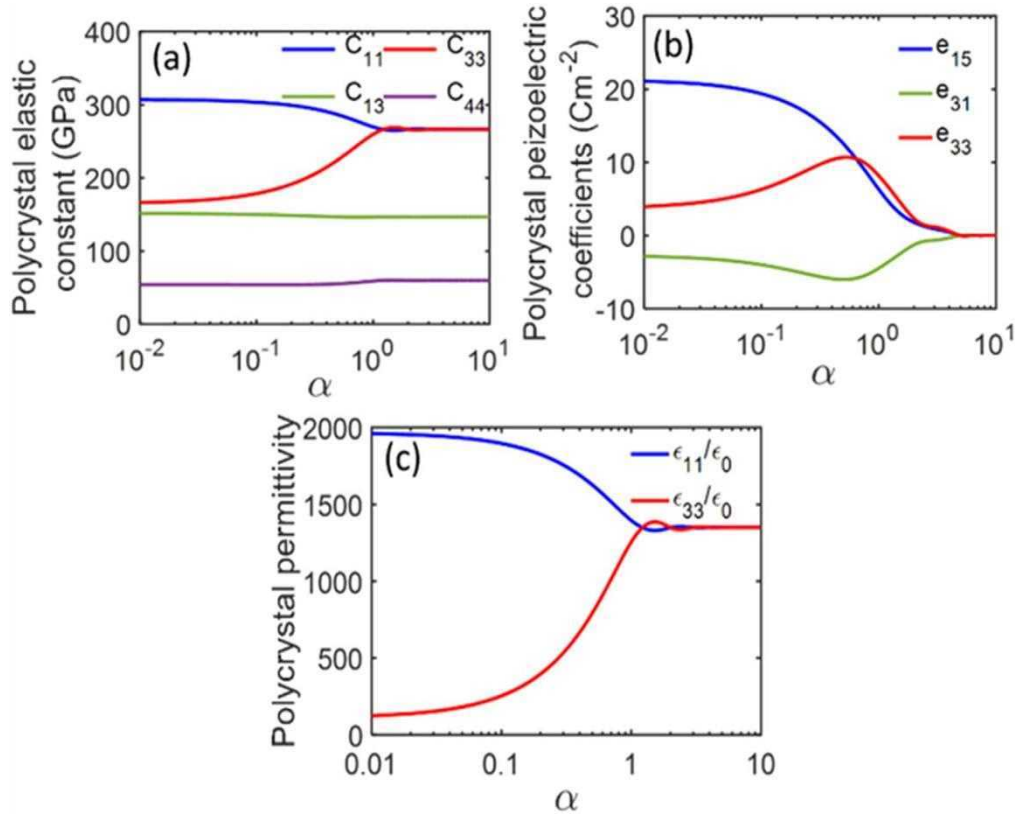


Figure A1. The effective electro-elastic coefficients of polycrystalline BaTiO₃, (a) the elastic coefficients, (b) the piezoelectric coefficients, (c) the relative permittivity.

Appendices

A1: The electroelastic coefficients of polycrystalline BaTiO₃

As mentioned in the section 2.2 of the paper, the piezoelectric inclusions are polycrystalline. Assuming the composites are poled in x_3 direction, polycrystallinity in this context refers to the randomness in the orientation of the BaTiO₃ unit cell dipoles around the direction of poling. The average orientation is quantified by a parameter α [26]. When $\alpha \rightarrow 0$, most of the dipoles are oriented along the poling direction and the sample appears to be single-crystal-line. When $\alpha \rightarrow \infty$, dipoles are randomly oriented and thus there is no net piezoelectric flux generation. In the [26], the effective electro-elastic properties of polycrystalline BaTiO₃ are calculated by computing orientational averages assuming a Gaussian distribution of orientations, characterized by the parameter α . The effective electro-elastic coefficients generated this way are shown in figure A1(a)–(c)

A2: Boundary conditions and effective electro-elastic coefficients of the composites

The boundary conditions BC1 and BC2 are used to obtain the effective elastic and piezoelectric coefficients of the composite [24, 25]. The table A1 lists the boundary conditions and the effective coefficients that are obtained by their application.

Table A1. Boundary conditions and corresponding effective properties.

Boundary condition	Effective property calculated
BC1	c_{11} , c_{13} , e_{31}
BC2	c_{33} , c_{13}

As shown in figures 1(a) and (b), the boundary conditions ensure that the average electric field in the composite is zero. Further, BC1 and BC2 force the following volume averages on the composite

- (a) BC1: $\epsilon_{11} = \epsilon_a$, $\epsilon_{33} = 0$
- (b) BC2: $\epsilon_{11} = 0$, $\epsilon_{33} = \epsilon_a$.

This allows us to compute the effective parameters as follows

- (a) On application of BC1

$$c_{11}^{eff} = \frac{\sigma_{11}}{\epsilon_a}, \quad c_{13}^{eff} = \frac{\sigma_{33}}{\epsilon_a}, \quad e_{31}^{eff} = \frac{D_3}{\epsilon_a}. \quad (A.1)$$

- (b) On application of BC2:

$$c_{33}^{eff} = \frac{\sigma_{33}}{\epsilon_a}, \quad c_{13}^{eff} = \frac{\sigma_{33}}{\epsilon_a}, \quad e_{33}^{eff} = \frac{D_3}{\epsilon_a}. \quad (A.2)$$

Table A2. The boundary conditions to compute the effective properties of the microstructured matrices. Note that ϵ_0 is the absolute permittivity of vacuum, and that ϵ_{11}^{eff} and ϵ_{33}^{eff} are the effective components of the relative permittivity of the homogenized matrix.

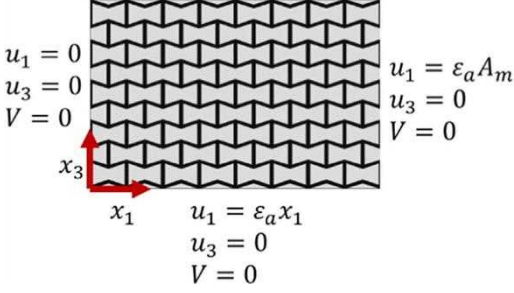
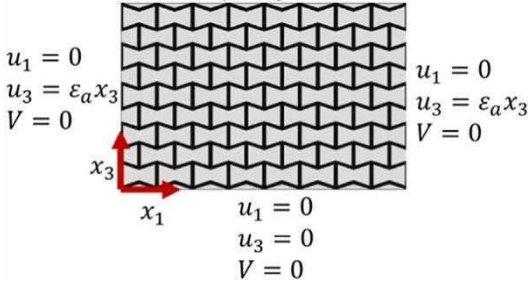
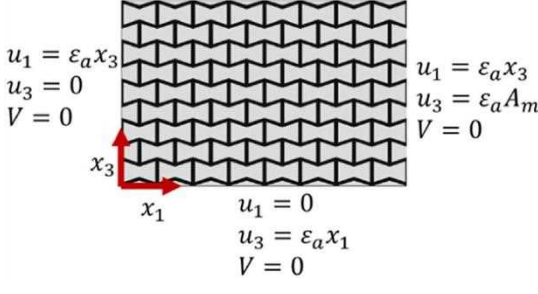
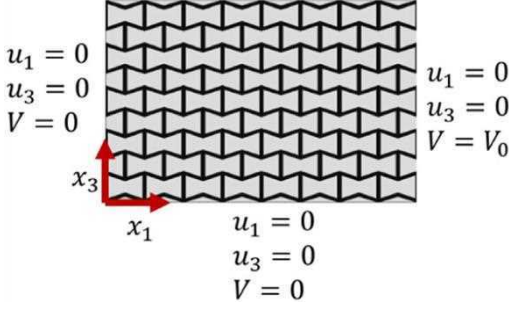
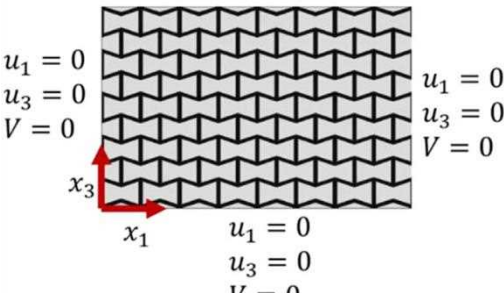
Boundary conditions	Effective property calculation
 <p> $u_1 = \epsilon_a x_1$ $u_3 = 0$ $V = 0$ $u_1 = 0$ $u_3 = 0$ $V = 0$ $u_1 = \epsilon_a A_m$ $u_3 = 0$ $V = 0$ $u_1 = \epsilon_a x_1$ $u_3 = 0$ $V = 0$ </p>	$c_{11}^{eff} = \frac{\sigma_{11}}{\epsilon_a}$ $c_{13}^{eff} = \frac{\sigma_{33}}{\epsilon_a}$
 <p> $u_1 = 0$ $u_3 = \epsilon_a B_m$ $V = 0$ $u_1 = 0$ $u_3 = \epsilon_a x_3$ $V = 0$ $u_1 = 0$ $u_3 = \epsilon_a x_3$ $V = 0$ $u_1 = 0$ $u_3 = 0$ $V = 0$ </p>	$c_{33}^{eff} = \frac{\sigma_{33}}{\epsilon_a}$ $c_{13}^{eff} = \frac{\sigma_{11}}{\epsilon_a}$
 <p> $u_1 = \epsilon_a x_3$ $u_3 = \epsilon_a x_1$ $V = 0$ $u_1 = \epsilon_a x_3$ $u_3 = 0$ $V = 0$ $u_1 = \epsilon_a x_3$ $u_3 = \epsilon_a A_m$ $V = 0$ $u_1 = 0$ $u_3 = \epsilon_a x_1$ $V = 0$ </p>	$c_{44}^{eff} = \frac{\sigma_{13}}{2\epsilon_a}$
 <p> $u_1 = 0$ $u_3 = 0$ $V = 0$ $u_1 = 0$ $u_3 = 0$ $V = 0$ $u_1 = 0$ $u_3 = 0$ $V = V_0$ $u_1 = 0$ $u_3 = 0$ $V = 0$ </p>	$\epsilon_{11}^{eff} = \frac{D_1}{\left(-\frac{V_0}{A_m}\right)\epsilon_0}$

Table A2. (Continued.)

Boundary conditions	Effective property calculation
$ \begin{aligned} u_1 &= 0 \\ u_3 &= 0 \\ V &= V_0 \end{aligned} $ 	$ \epsilon_{33}^{eff} = \frac{D_3}{\left(-\frac{V_0}{B_m}\right)\epsilon_0} $

A3: The boundary conditions to determine the effective elastic and permittivity coefficients of the microstructured matrices

We provide the details of the boundary conditions used to calculate the boundary conditions of the matrices illustrated in figures 4(a), (b). These materials are non-piezoelectric and hence the equations (1)–(2) are solved assuming $e_{ijk} = 0$, i.e. the coupling between the electric and elastic fields is removed. Table A2 provides the boundary conditions and the corresponding calculations to obtain the effective properties. These are standard boundary conditions used for obtaining the effective electro-elastic properties by homogenization. While the illustrations show the boundary conditions being applied to the auxetic matrix RVE, the nonauxetic matrix is also subject to the same conditions.

ORCID iDs

Jagdish A Krishnaswamy  <https://orcid.org/0000-0001-7451-3237>

Luis Rodriguez-Tembleque  <https://orcid.org/0000-0003-2993-8361>

References

- [1] Safaei M, Sodano H A and Anton S R 2019 A review of energy harvesting using piezoelectric materials: state-of-the-art a decade later (2008–2018) *Smart Mater. Struct.* (<https://doi.org/10.1088/1361-665X/ab36e4>)
- [2] Bowen C R, Topolov V Y, Zhang Y and Panich A A 2018 1-3-Type composites based on ferroelectrics: electromechanical coupling, figures of merit, and piezotechnical energy-harvesting applications *Energy Technol.* **6** 813–28
- [3] Cui H, Hensleigh R, Yao D, Maurya D, Kumar P, Kang M G, Priya S and Zheng X R 2019 Three-dimensional printing of piezoelectric materials with designed anisotropy and directional response *Nat. Mater.* **18** 234
- [4] Lakes R 1993 Materials with structural hierarchy *Nature* **361** 511
- [5] Agnelli F, Constantinescu A and Nika G 2018 Optimal design of auxetic, additively manufactured, polymeric structures *arXiv:1809.02467v1*
- [6] Kim K, Zhu W, Qu X, Aaronson C, McCall W R, Chen S and Sirbulu D J 2014 3D optical printing of piezoelectric nanoparticle–polymer composite materials *ACS Nano* **8** 9799–806
- [7] Phatharapeetranun N, Ksapabutr B, Marani D, Bowen J R and Esposito V 2017 3D-printed barium titanate/poly-(vinylidene fluoride) nano-hybrids with anisotropic dielectric properties *J. Mater. Chem. C* **5** 12430–40
- [8] Ibn-Mohammed T, Koh S, Reaney I, Sinclair D, Mustapha K, Acquaye A and Wang D 2017 Are lead-free piezoelectrics more environmentally friendly? *MRS Commun.* **7** 1–7
- [9] Maurya D, Peddigari M, Kang M-G, Geng L D, Sharpes N, Annappureddy V, Palneedi H, Sriramdas R, Yan Y and Song H-C 2018 Lead-free piezoelectric materials and composites for high power density energy harvesting *J. Mater. Res.* **33** 2235–63
- [10] Kim H, Torres F, Islam M T, Islam M D, Chavez L A, Rosales C A G, Wilburn B R, Stewart C M, Noveron J C and Tseng T-L B 2017 Increased piezoelectric response in functional nanocomposites through multiwall carbon nanotube interface and fused-deposition modeling three-dimensional printing *MRS Commun.* **7** 960–6
- [11] Park K I, Lee M, Liu Y, Moon S, Hwang G T, Zhu G, Kim J E, Kim S O, Kim D K and Wang Z L 2012 Flexible nanocomposite generator made of BaTiO₃ nanoparticles and graphitic carbons *Adv. Mater.* **24** 2999–3004
- [12] Krishnaswamy J A, Buroni F C, Garcia-Sanchez F, Melnik R V N, Rodriguez-Tembleque L and Saez A 2019 Lead-free piezocomposites with CNT-modified matrices: accounting for agglomerations and molecular defects *Compos. Struct.* **224** 111033
- [13] Lakes R S 2017 Negative-Poisson's-ratio materials: auxetic solids *Annu. Rev. Mater. Res.* **47** 63–81
- [14] Alderson A and Alderson K 2007 Auxetic materials *Proc. Inst. Mech. Eng. G* **221** 565–75
- [15] Evans K E and Alderson A 2000 Auxetic materials: functional materials and structures from lateral thinking! *Adv. Mater.* **12** 617–28
- [16] Reid D R, Pashine N, Bowen A S, Nagel S R and de Pablo J J 2019 Ideal isotropic auxetic networks from random networks *Soft Matter* **15** 8084–91

- [17] Liu Y and Hu H 2010 A review on auxetic structures and polymeric materials *Sci. Res. Essays* **5** 1052–63
- [18] Ha C S, Plesha M E and Lakes R S 2016 Chiral three-dimensional lattices with tunable Poisson's ratio *Smart Mater. Struct.* **25** 054005
- [19] Körner C and Liebold-Ribeiro Y 2014 A systematic approach to identify cellular auxetic materials *Smart Mater. Struct.* **24** 025013
- [20] Li Q, Kuang Y and Zhu M 2017 Auxetic piezoelectric energy harvesters for increased electric power output *AIP Adv.* **7** 015104
- [21] Topolov V Y and Bowen C R 2015 High-performance 1–3-type lead-free piezo-composites with auxetic polyethylene matrices *Mater. Lett.* **142** 265–8
- [22] Qin R-S, Xiao Y and Lan H 2014 Numerical simulation of effective properties of 3d piezoelectric composites *J. Eng.* **2014** 824806
- [23] Iyer S, Alkhader M and Venkatesh T 2015 Electromechanical behavior of auxetic piezoelectric cellular solids *Scr. Mater.* **99** 65–8
- [24] Saputra A A, Sladek V, Sladek J and Song C 2018 Micromechanics determination of effective material coefficients of cement-based piezoelectric ceramic composites *J. Intell. Mater. Syst. Struct.* **29** 845–62
- [25] Sladek J, Sladek V, Krahulec S and Song C 2016 Micromechanics determination of effective properties of voided magneto-electroelastic materials *Comput. Mater. Sci.* **116** 103–12
- [26] Li J Y 2000 The effective electroelastic moduli of textured piezoelectric polycrystalline aggregates *J. Mech. Phys. Solids* **48** 529–52
- [27] Alderson K, Webber R, Kettle A and Evans K 2005 Novel fabrication route for auxetic polyethylene: I. Processing and microstructure *Polym. Eng. Sci.* **45** 568–78
- [28] Webber R, Alderson K and Evans K 2008 A novel fabrication route for auxetic polyethylene: II. Mechanical properties *Polym. Eng. Sci.* **48** 1351–8
- [29] Turturro M V, Sokic S, Larson J C and Papavasiliou G 2013 Effective tuning of ligand incorporation and mechanical properties in visible light photopolymerized poly (ethylene glycol) diacrylate hydrogels dictates cell adhesion and proliferation *Biomed. Mater.* **8** 025001
- [30] Noda N and Obrzut J 2002 High frequency dielectric relaxation in polymers filled with ferroelectric ceramics *Materials Research Society Symp. Proc.* vol 698
- [31] Raponi O d A, Raponi R d A, Barban G B, Benedetto R M D and Ancelotti Junior A C 2017 Development of a simple dielectric analysis module for online cure monitoring of a commercial epoxy resin formulation *Mater. Res.* **20** 291–7
- [32] Berlincourt D and Jaffe H 1958 Elastic and piezoelectric coefficients of single-crystal barium titanate *Phys. Rev.* **111** 143
- [33] Yamada T, Ueda T and Kitayama T 1982 Piezoelectricity of a high-content lead zirconate titanate/polymer composite *J. Appl. Phys.* **53** 4328–32
- [34] Hori M and Nemat-Nasser S 1999 On two micromechanics theories for determining micro–macro relations in heterogeneous solids *Mech. Mater.* **31** 667–82
- [35] Tian W, Qi L, Chao X, Liang J and Fu M 2019 Periodic boundary condition and its numerical implementation algorithm for the evaluation of effective mechanical properties of the composites with complicated microstructures *Composites B* **162** 1–10
- [36] Berger H, Kari S, Gabbert U, Rodriguez-Ramos R, Bravo-Castillero J, Guinovart-Diaz R, Sabina F and Maugin G 2006 Unit cell models of piezoelectric fiber composites for numerical and analytical calculation of effective properties *Smart Mater. Struct.* **15** 451
- [37] Suquet P M 1985 Elements of homogenization for inelastic solid mechanics, homogenization techniques for composite media *Lect. Notes Phys.* **272** 193
- [38] Dirrenberger J, Forest S and Jeulin D 2013 Effective elastic properties of auxetic microstructures: anisotropy and structural applications *Int. J. Mech. Mater. Des.* **9** 21–33
- [39] Krishnaswamy J A, Buroni F C, Garcia-Sanchez F, Melnik R V N, Rodriguez-Tembleque L and Saez A 2019 Improving the performance of lead-free piezoelectric composites by using polycrystalline inclusions and tuning the dielectric matrix environment *Smart Mater. Struct.* **28** 075032